BULLETIN OF THE POLISH ACADEMY OF SCIENCES
TECHNICAL SCIENCES, Vol. 63, No. 2, 2015
DOI: 10.1515/bpasts-2015-0058

Effects of inclined magnetic field and Joule heating in mixed convective peristaltic transport of non-Newtonian fluids

F.M. ABBASI[1]*, T. HAYAT[2,3], and A. ALSAEDI[3]

[1] Department of Mathematics, Comsats Institute of Information Technology, Islamabad 44000, Pakistan
[2] Department of Mathematics, Quaid-I-Azam University 45320, Islamabad 44000, Pakistan
[3] Nonlinear Analysis and Applied Mathematics (NAAM) Research Group, Faculty of Science, King Abdulaziz University, Jeddah 21589, Saudi Arabia

Abstract. This article describes the influence of an inclined magnetic field on the mixed convective peristaltic transport of fluid in an inclined channel. Two types of non-Newtonian fluids are considered. The problem formulation is presented for the Eyring-Prandtl and Sutterby fluids. Viscous dissipation and Joule heating in the heat transfer process are retained. The presence of a heat source in the energy equation is ensured. The resulting problems are solved by the perturbation method. The plots for different parameters of interest are given and discussed. Numerical values of a heat transfer rate are given and analyzed.

Key words: mixed convection, eyring-prandtl fluid, sutterby fluid, inclined magnetic field.

1. Introduction

The peristaltic transport of fluid is a current topic in fluid dynamics research for the interests in the practical as well as academic sense. It has received special attention of the modelers and numerical simulationalists. Such an interest of the investigators can be estimated because of a wide coverage of peristaltic motion in engineering and medical industry. Generally, the biofluids are propelled in ducts by means of progressive waves along the ducts by walls. In particular, chyme movement in the entire gastrointestinal tract, urine through the ureter, ovum in the female fallopian tube, vasomotion of small blood vessels, spermatozoa in cervical canal, bile in bile duct and transport of food grains and liquids from the mouth through the oesophagus represent peristalsis in the physiological world. The industrial applications of peristalsis include sanitary fluid transport, blood pumps in heart lung machine, corrosive fluids transport and toxic liquid transport in nuclear industry. The locomotion of worms and translocation of water in tall trees is also due to principle of peristalsis. Further, design of several modern medical devices is based upon peristaltic pumping for fluid transport without internal moving parts. Motivated by such applications, extensive studies have been made for peristaltic flows of hydrodynamic viscous fluids in a planar channel. All such investigations are performed through one or more assumptions of long wavelength, low Reynolds number, small wave number, small amplitude ratio etc. Latham [1] and Shapiro et al. [2] presented pioneering researches on the peristaltic motion of viscous fluid. Afterwards even reasonable attention has been given to discuss the peristaltic transport of non-Newtonian fluids in a planar channel. Some advancement in this direction is also made for peristaltic transport of magnetohydrodynamic (MHD) viscous/non-Newtonian fluids in the presence of an applied magnetic field. Such motivation in fact stems due to applications of magnetohydrodynamic flows in MHD generators, MHD pumps and accelerators, hyperthermia, reduction of bleeding during surgery, cancer tumor treatment, removal of blockage in the arteries, aerodynamic heating process, polymer technology, electrostatic precipitation and in the molten metals purification from non-metallic inclusions and fluid droplet sprays. In oxygenation and hemodialysis processes, cryosurgery, localized tumor therapy and therapy of anticancer treatment, the impact of heat transfer is further significant. The previous contributions in the literature show that MHD peristaltic flows have been studied in the presence of applied magnetic field/heat transfer. Some significant recent researches in this direction has included the attempts [3–15] and many references therein.

The published studies about the mixed convective peristaltic MHD flows of non-Newtonian fluids are still scarce. Such investigations are further narrowed down when an inclined magnetic field and Joule heating effects are taken into account. The study of the Joule heating and inclined magnetic field effects in mixed convective peristaltic flow of non-Newtonian fluids in an inclined channel is still very incipient. Hence the motivation of the present communication is to contribute to the yet incipient study of MHD mixed convective peristaltic flow of two types of non-Newtonian fluids in a symmetric channel with Joule heating. Both applied magnetic field and channel are taken inclined. The constitutive equations of Eyring-Prandtl and Sutterby fluids are used in the mathematical modelling. Long wavelength and low Reynolds number approach is followed. The series solutions are constructed and analysis of physical quantities is given through plots. Numerical values of a heat transfer rate are computed and examined.

*e-mail: abbasisarkar@gmail.com

2. Mathematical formulation

We consider the peristaltic transport of non-Newtonian fluids in a symmetric channel inclined at an angle α. A uniform magnetic field of strength B_0 is incident at an angle β. The wave propagating along the wall of symmetric channel is

$$\overline{H}(\overline{X}, \overline{t}) = a + \varepsilon,$$

where a is the half channel width and ε is the disturbance produced due to propagation of peristaltic waves at the walls. This disturbance can be written in the form

$$\varepsilon = b\cos\left(\frac{2\pi}{\lambda}(\overline{X} - c\overline{t})\right),$$

in which $\overline{t}$ is time, b is the amplitude of the peristaltic wave, c and λ are the speed and wavelength of the waves respectively. Appropriate velocity field for this problem in laboratory frame is $\overline{V} = \left[U(\overline{X}, \overline{Y}, \overline{t}),\, V(\overline{X}, \overline{Y}, \overline{t}),\, 0\right]$.

Basic laws of conservation of mass and momentum for the flow analysis under consideration are

$$\overline{\nabla}.\overline{V} = 0, \tag{1}$$

$$\begin{aligned}\rho\frac{d\overline{U}}{dt} &= -\frac{\partial\overline{P}}{\partial\overline{X}} + \frac{\partial\overline{\tau}_{\overline{X}\overline{X}}}{\partial\overline{X}} + \frac{\partial\overline{\tau}_{\overline{X}\overline{Y}}}{\partial\overline{Y}}\\ &-\sigma B_0^2\cos\beta\left(\overline{U}\cos\beta - \overline{V}\sin\beta\right)\\ &+\rho g\alpha^*\left(T - T_0\right)\sin\alpha + \rho g\sin\alpha,\end{aligned} \tag{2}$$

$$\begin{aligned}\rho\frac{d\overline{V}}{dt} &= -\frac{\partial\overline{P}}{\partial\overline{Y}} + \frac{\partial\overline{\tau}_{\overline{Y}\overline{X}}}{\partial\overline{X}} + \frac{\partial\overline{\tau}_{\overline{Y}\overline{Y}}}{\partial\overline{Y}}\\ &-\sigma B_0^2\sin\beta\left(\overline{U}\cos\beta - \overline{V}\sin\beta\right)\\ &-\rho g\alpha^*\left(T - T_0\right)\cos\alpha - \rho g\cos\alpha,\end{aligned} \tag{3}$$

in which ρ is the density of fluid, $\overline{P}$ the pressure, $\overline{\boldsymbol{\tau}}$ the extra stress tensor, g the acceleration due to gravity, σ the electric conductivity, T the temperature, T_0 the temperature of the wall and α^* the thermal expansion coefficient. The energy equation can be expressed as

$$\begin{aligned}\rho C_p\frac{dT}{dt} &= K\left[T_{\overline{X}\overline{X}} + T_{\overline{Y}\overline{Y}}\right]\\ &+\overline{\boldsymbol{\tau}}.\overline{L} + \sigma B_0^2\left(\overline{U}\cos\beta - \overline{V}\sin\beta\right)^2 + \gamma.\end{aligned} \tag{4}$$

Here C_p is the specific heat, K the thermal conductivity, $\overline{\boldsymbol{\tau}}.\overline{L}$ the viscous dissipation term and γ the heat source/sink parameter.

We consider $(\overline{u}, \overline{v})$ and $\overline{p}$ as the velocity components and pressure in the wave frame $(\overline{x}, \overline{y})$. The transformations between laboratory and wave frames are

$$\begin{aligned}\overline{x} &= \overline{X} - c\overline{t}, \qquad \overline{y} = \overline{Y},\\ \overline{u} &= \overline{U} - c, \qquad \overline{v} = \overline{V},\\ \overline{p}(\overline{x}, \overline{y}) &= \overline{P}(\overline{X}, \overline{Y}, \overline{t}).\end{aligned} \tag{5}$$

The equations in wave frame can be expressed as follows:

$$\frac{\partial\overline{u}}{\partial\overline{x}} + \frac{\partial\overline{v}}{\partial\overline{y}} = 0, \tag{6}$$

$$\begin{aligned}&\rho\left((\overline{u}+c)\,\frac{\partial}{\partial\overline{x}} + \overline{v}\frac{\partial}{\partial\overline{y}}\right)(\overline{u}+c)\\ &= -\frac{\partial\overline{p}}{\partial\overline{x}} + \frac{\partial\overline{\tau}_{\overline{x}\overline{x}}}{\partial\overline{x}} + \frac{\partial\overline{\tau}_{\overline{x}\overline{y}}}{\partial\overline{y}}\\ &-\sigma B_0^2\cos\beta\left((\overline{u}+c)\cos\beta - \overline{v}\sin\beta\right)\\ &+\rho g\alpha^*\left(T - T_0\right)\sin\alpha + \rho g\sin\alpha,\end{aligned} \tag{7}$$

$$\begin{aligned}&\rho\left((\overline{u}+c)\,\frac{\partial}{\partial\overline{x}} + \overline{v}\frac{\partial}{\partial\overline{y}}\right)\overline{v}\\ &= -\frac{\partial\overline{p}}{\partial\overline{y}} + \frac{\partial\overline{\tau}_{\overline{y}\overline{x}}}{\partial\overline{x}} + \frac{\partial\overline{\tau}_{\overline{y}\overline{y}}}{\partial\overline{y}}\\ &-\sigma B_0^2\sin\beta\left((\overline{u}+c)\cos\beta - \overline{v}\sin\beta\right)\\ &-\rho g\alpha^*\left(T - T_0\right)\cos\alpha - \rho g\cos\alpha,\end{aligned} \tag{8}$$

$$\begin{aligned}&\rho C_p\left((\overline{u}+c)\,T_{\overline{x}} + \overline{v}T_y\right) = K\left[T_{\overline{x}\overline{x}} + T_{\overline{y}\overline{y}}\right] + \upsilon\left(\overline{\tau}.\overline{L}\right)\\ &+\sigma B_0^2\left((\overline{u}+c)\cos\beta - \overline{v}\sin\beta\right)^2 + \gamma.\end{aligned} \tag{9}$$

We now introduce the dimensionless quantities as

$$\begin{aligned}x &= \frac{\overline{x}}{\lambda}, \qquad y = \frac{\overline{y}}{a}, \qquad u = \frac{\overline{u}}{c},\\ v &= \frac{\overline{v}}{c\delta}, \qquad \delta = \frac{a}{\lambda}, \qquad h = \frac{H}{a},\\ d &= \frac{b}{a}, \qquad p = \frac{a^2\overline{p}}{c\lambda\eta_0}, \qquad \theta = \frac{T - T_0}{T_0},\\ M^2 &= \left(\frac{\sigma}{\eta_0}\right)B_0^2a^2, \qquad \mathrm{Re} = \frac{\rho ca}{\eta_0}, \qquad t = \frac{c\overline{t}}{\lambda},\\ Br &= \underset{E}{\mathrm{Pr}}, \qquad E = \frac{c^2}{C_pT_0},\\ \mathrm{Pr} &= \frac{\eta_0C_p}{K}, \qquad Gr = \frac{\rho g\alpha^*T_0a^2}{\eta_0c},\\ \phi &= \frac{a^2\gamma}{KT_0}, \qquad \boldsymbol{\tau} = \frac{a\overline{\boldsymbol{\tau}}_{xy}}{c\eta_0}m = M\cos\beta,\\ u &= \frac{\partial\psi}{\partial y}, \qquad v = -\frac{\partial\psi}{\partial x},\end{aligned} \tag{10}$$

where Re is the Reynolds number, M the Hartman number, Br the Brinkman number, E the Eckert number, Pr the Prandtl number, δ the wave number, ψ the stream function, η_0 the viscosity at zero shear rate, Gr the local Grashoff number, ϕ dimensionless heat source/sink parameter, θ the dimensionless temperature and incompressibility condition is automatically satisfied.

We seek to analyze the behavior of two separate non-Newtonian fluids namely Eyring-Prandtl and Sutterby fluids. The corresponding extra stress tensors of these models are:
Eyring Prandtl [16]

$$\overline{\boldsymbol{\tau}} = \left[\frac{A^*\eta_0\,\mathrm{arcsin}\,h\left[\frac{\left|\xi\left(\overline{V}\right)\right|}{B^*}\right]}{\left|\xi\left(\overline{V}\right)\right|}\right]\xi\left(\overline{V}\right) \tag{11}$$

and Sutterby fluid [17]

$$\overline{\boldsymbol{\tau}} = \left[\frac{\eta_0\,\mathrm{arcsin}\,h\left[B^{**}\left|\xi\left(\overline{V}\right)\right|\right]}{B^{**}\left|\xi\left(\overline{V}\right)\right|}\right]^{A^{**}}\xi\left(\overline{V}\right), \tag{12}$$

where $\xi\left(\overline{V}\right)$ denotes the symmetric part of the velocity gradient, A^*, A^{**}, B^* and B^{**} are the material constants for the respective fluid models. Upon simplification the corresponding dimensionless tensor components yield

$$\boldsymbol{\tau}_{xy} = \left\{A - B\left(\psi_{yy}\right)^2\right\}\psi_{yy}, \quad \text{Eyring-Prandtl,} \tag{13}$$

$$\boldsymbol{\tau}_{xy} = \left\{1 - B_1\left(\psi_{yy}\right)^2\right\}\psi_{yy}, \quad \text{Sutterby.} \tag{14}$$

In above equations A, B and B_1 are the dimensionless forms of the material constants given by

$$A = \frac{A^*}{B^*}, \quad B = \frac{Ac^2}{3!B^{*2}a^2}, \quad B_1 = \frac{A^{**}B^{**2}c^2}{3!a^2}.$$

Utilization of tensor components (Eqs. (13), (14)) and the dimensionless quantities from Eq. (10) into Eqs. (7)–(9) and then applying long wavelength and low Reynolds number approximations [18, 19], we have for Eyring-Prandtl fluid the following expressions:

$$p_x = \frac{\partial}{\partial y}\left\{A - B\left(\psi_{yy}\right)^2\right\}\psi_{yy} - m^2\left(\psi_y + 1\right) + Gr\theta\sin\alpha + \frac{\mathrm{Re}\sin\alpha}{Fr}, \tag{15}$$

$$p_y = 0, \tag{16}$$

$$\theta_{yy} + Br\left\{A\psi_{yy}^2 - B\left(\psi_{yy}\right)^4\right\} + Brm^2\left(\psi_y + 1\right)^2 + \mathrm{Pr}\phi = 0, \tag{17}$$

and for Sutterby fluid model we have

$$p_x = \frac{\partial}{\partial y}\left\{1 - B_1\left(\psi_{yy}\right)^2\right\}\psi_{yy} - m^2\left(\psi_y + 1\right) + Gr\theta\sin\alpha + \frac{\mathrm{Re}\sin\alpha}{Fr}, \tag{18}$$

$$p_y = 0, \tag{19}$$

$$\theta_{yy} + Br\left\{\psi_{yy}^2 - B_1\left(\psi_{yy}\right)^4\right\} + Brm^2\left(\psi_y + 1\right)^2 + \mathrm{Pr}\phi = 0. \tag{20}$$

Defining η and F as the dimensionless mean flows in the laboratory and wave frames we have

$$\eta = F + 1, \tag{21}$$

where

$$F = \int_0^h \frac{\partial\psi}{\partial y}dy. \tag{22}$$

The pressure rise per wavelength is

$$\Delta P_\lambda = \int_0^h \left(\frac{dp}{dx}\right)dx. \tag{23}$$

The subjected dimensionless boundary conditions are

$$\begin{aligned} &\psi = 0, \quad \psi_{yy} = 0, \quad \theta_y = 0, \quad \text{at} \quad y = 0, \\ &\psi = F, \quad \psi_y = -1, \quad \theta = 0, \quad \text{at} \quad y = h, \end{aligned} \tag{24}$$

with

$$h(x) = 1 + d\cos(2\pi x), \tag{25}$$

3. Series and numerical solutions

The resulting equations are coupled nonlinear equations. We seek the series solutions of the problem for which we expand the flow quantities in powers of Br and the non-Newtonian parameter $B(B_1)$ for Eyring-Prandtl (Sutterby) fluid (for Br, B, $B_1 < 1$) as follows:

$$\begin{aligned} \psi &= \psi_0 + Br\psi_1 + ... \\ F &= F_0 + BrF_1 + ... \\ p &= p_0 + Brp_1 + ... \end{aligned}$$

We expand

$$\begin{aligned} \psi_0 &= \psi_{00} + B\psi_{01} + ... \\ \psi_1 &= \psi_{10} + B\psi_{11} + ... \\ F_0 &= F_{00} + BF_{01} + ... \\ F_1 &= F_{10} + BF_{11} + ... \\ P_0 &= P_{00} + BP_{01} + ... \\ P_1 &= P_{10} + BP_{11} + ... \end{aligned}$$

and retain only up to first order of Br and B. Also numerical solutions to these problems are calculated using Shooting method in **Mathematica**. A comparison of both the results is made through tables at the end. Solutions obtained for the pressure rise, pressure gradient, stream function, longitudinal velocity and temperature are analyzed through graphs and tables in the next section.

4. Analysis of the results

Explicitly this section aims to analyze the obtained results via graphs. Results for both the fluid models are plotted and analyzed. A comparative study is also given. Graphs of pressure rise, pressure gradient, velocity profile, stream function and dimensionless temperature are plotted. Figures 1–15 are plotted for the Eyring-Prandtl fluid model and Figs. 16–29 for the Sutterby fluid.

Analysis of the Eyring-Prandtl fluid model

Figure 1 are plotted to examine the behavior of pressure rise versus the flow rate. It is noted that there exists a critical value of flow rate below which the value of pressure rise is positive and above that value it is positive. This critical value corresponds to the free pumping flux for which the pressure difference is zero (Ali et al. [5]). The value of Δp_λ increases with the increase in A, $\cos\beta$ and M in the peristaltic pumping region ($\Delta p_\lambda > 0$ and $\eta > 0$) and in retrograde pumping region ($\Delta p_\lambda > 0$ and $\eta < 0$) whereas it decreases in the augmented pumping region ($\Delta p_\lambda < 0$ and $\eta > 0$). The behavior of pressure rise is exactly reverse for the case of increasing M.

Figure 2 are plotted for the analysis of pressure gradient for changing values of embedded parameters. Pressure gradient showed wave like behavior which may be due to peristalsis. Pressure gradient is observed to decrease with increase in M and Fr but it increases when inclination angle α, β, Re and Gr are increased. For all these parameters the maximum value of the pressure gradient was found to occur at the center of the channel. For small values of A, the value of pressure gradient is maximum near the end points of the

wave (i.e. more occluded part) and when the value of A is increased then maximum value occurs in the wider part of the channel (see Fig. 2f). Impact of B on the pressure gradient is opposite to that of A i.e. as B increases the maximum value of the pressure gradient shifts from wider to the narrow part of the channel (see Fig. 2g).

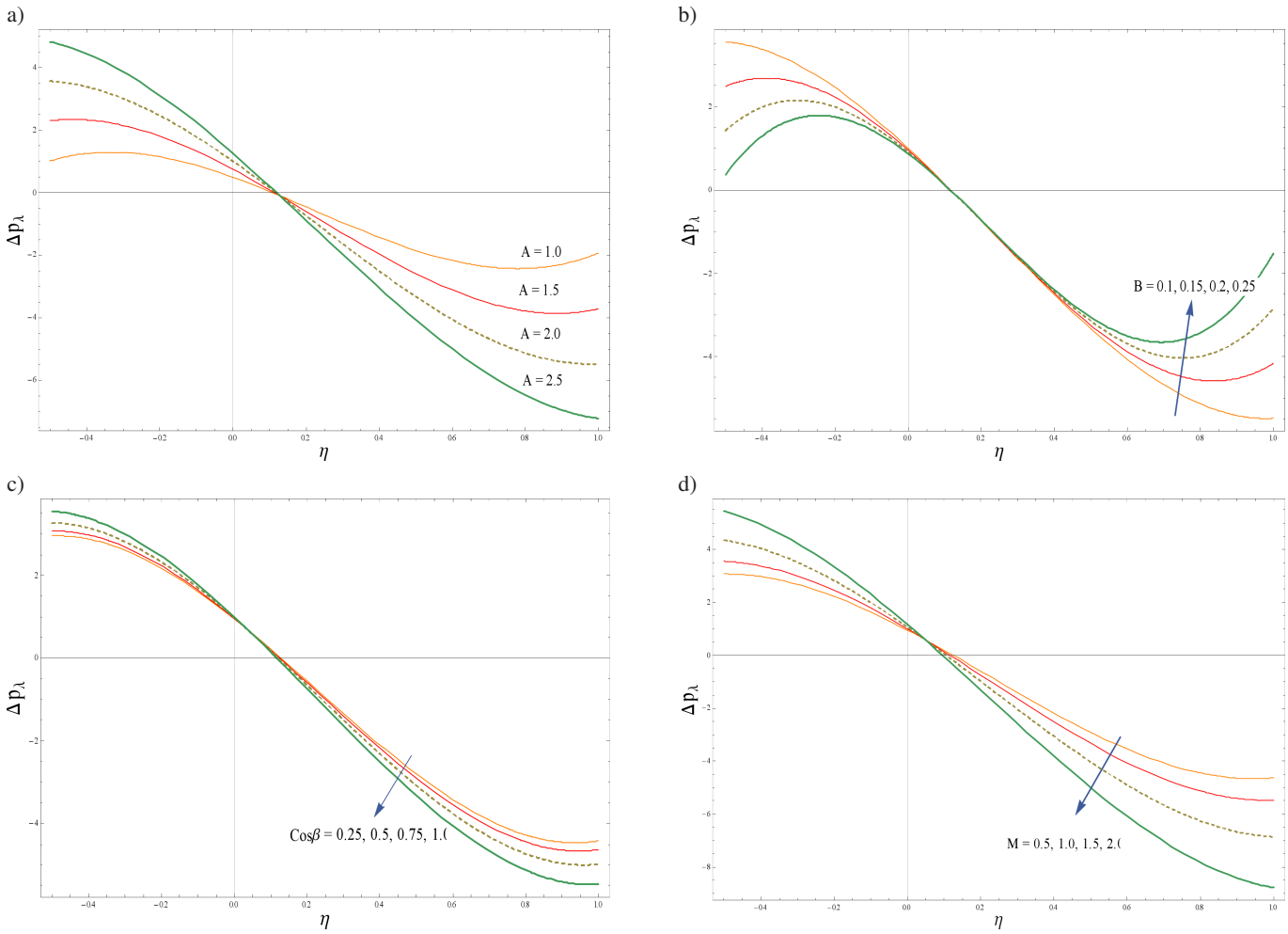

Fig. 1. Variation of pressure rise with different parameters

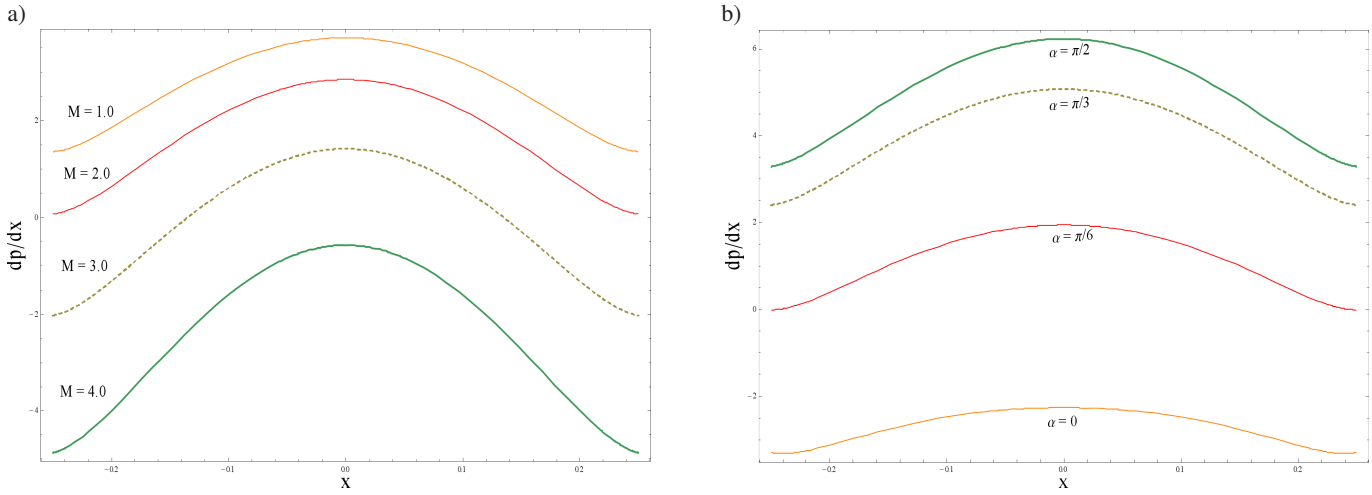

[Fig. 2ab]

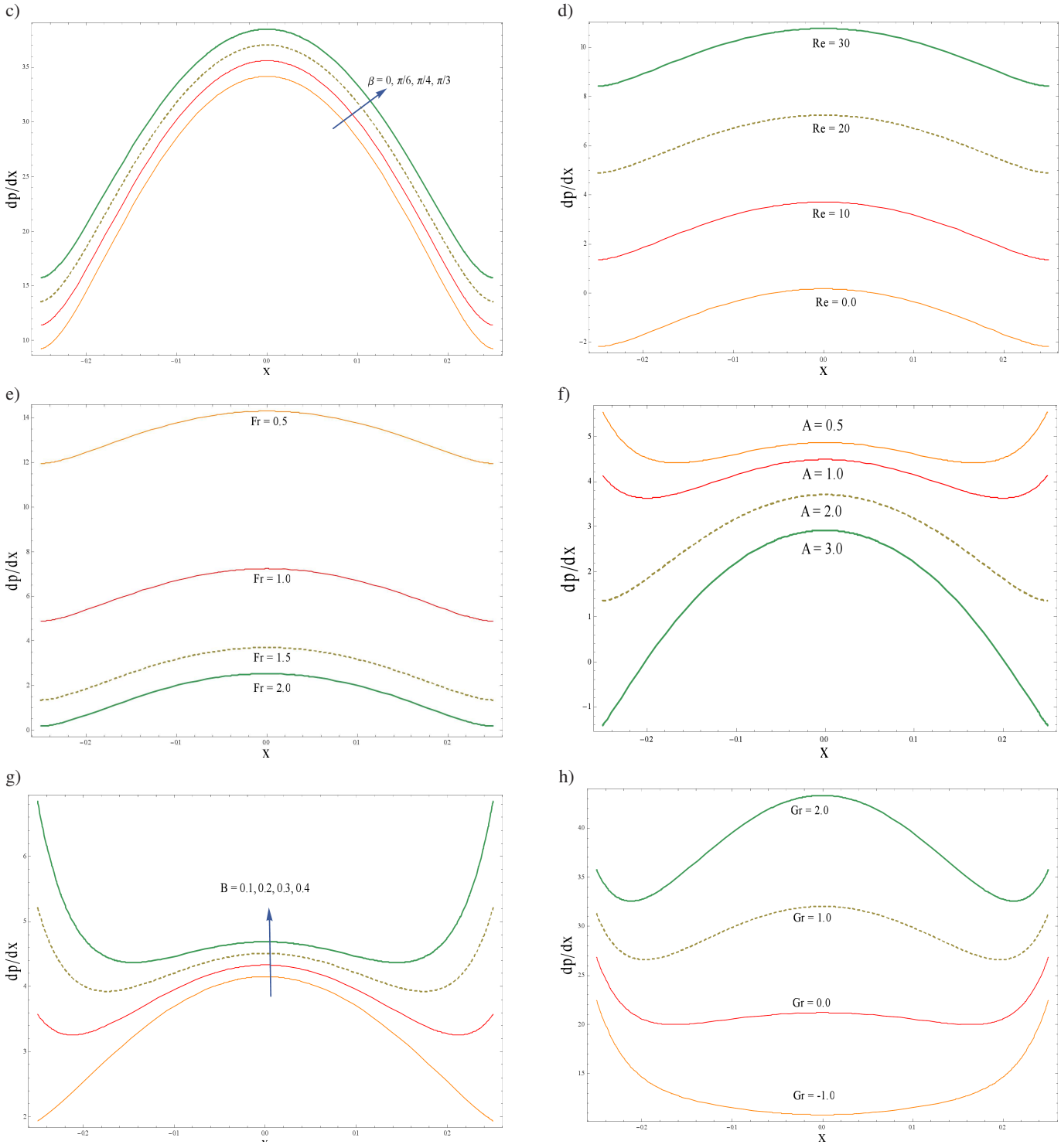

Fig. 2. Variation of pressure gradient with different parameters

Figures 3–7 are plotted to examine the change in streamlines with varying parametric values. It is seen that the size of trapped bolus decreases by increasing M and B whereas it increases for larger A and β. Moreover the effects of M and B on the streamlines is more prominent than that of A and β. The inclination angle α has very small effect on the streamlines.

The longitudinal velocity is seen to observe parabolic trajectory with maximum value near the center of the channel in all the graphs. The maximum value was found to decrease with an increase in M and B but it increases when A and Gr are enhanced. The channel inclination α and magnetic field inclination β when varied between 0 and $\pi/2$ tend to increase the maximum value of the velocity. Moreover, as the value of B is increased it forbids the velocity to attain maximum value near the center of the channel (see Fig. 8).

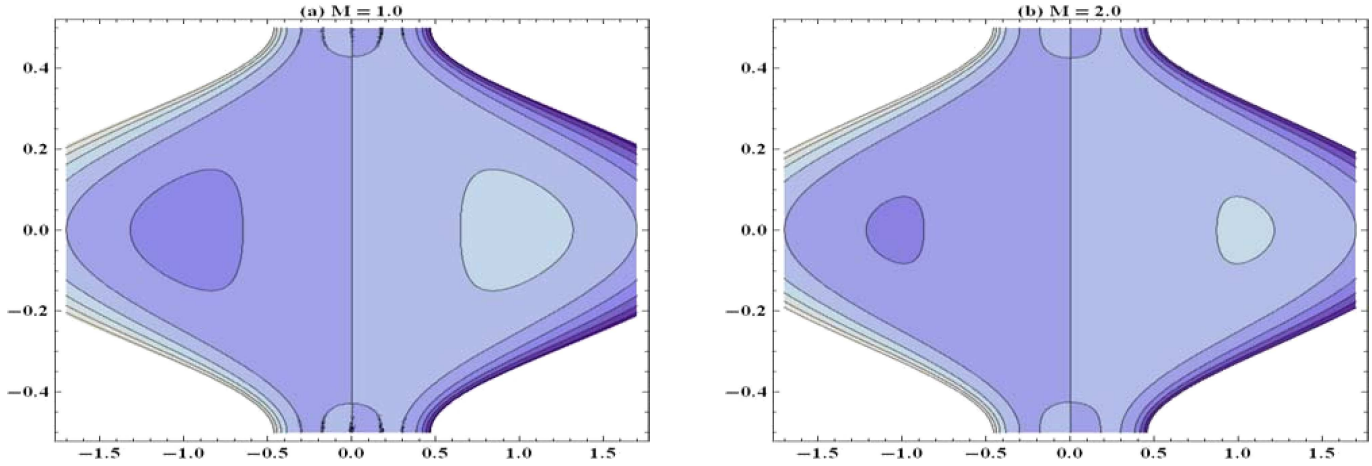

Fig. 3. Streamlines for Hartman number M

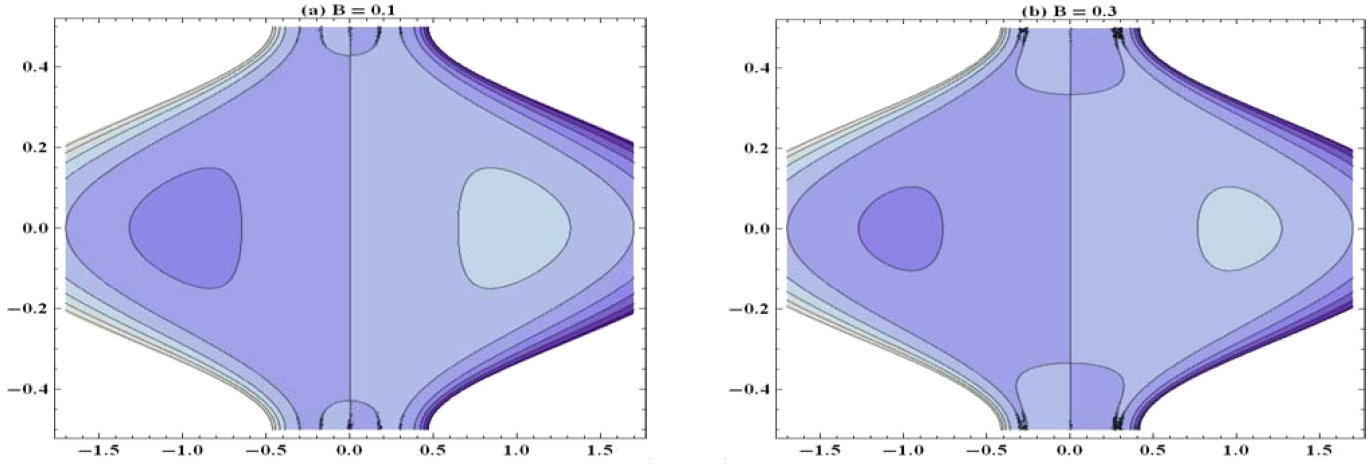

Fig. 4. Streamlines for non-Newtonian parameter B

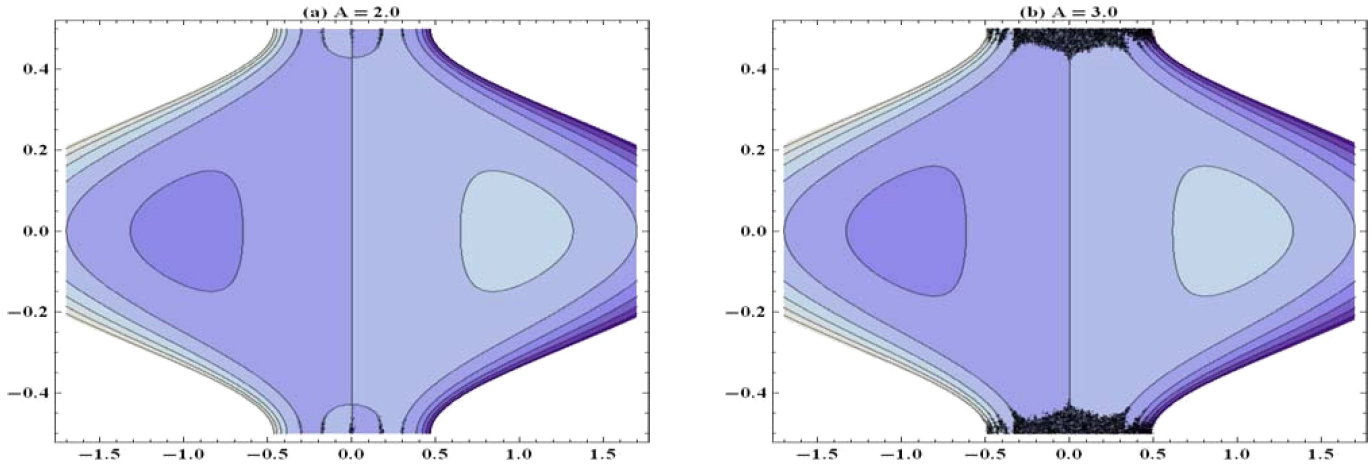

Fig. 5. Streamlines for non-Newtonian parameter A

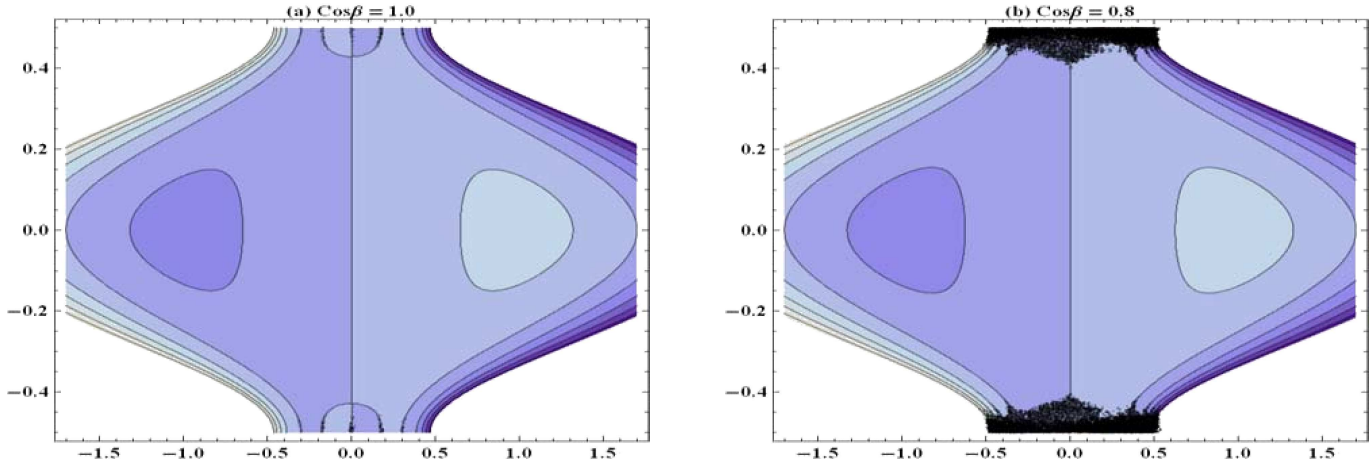

Fig. 6. Streamlines for magnetic field inclination β

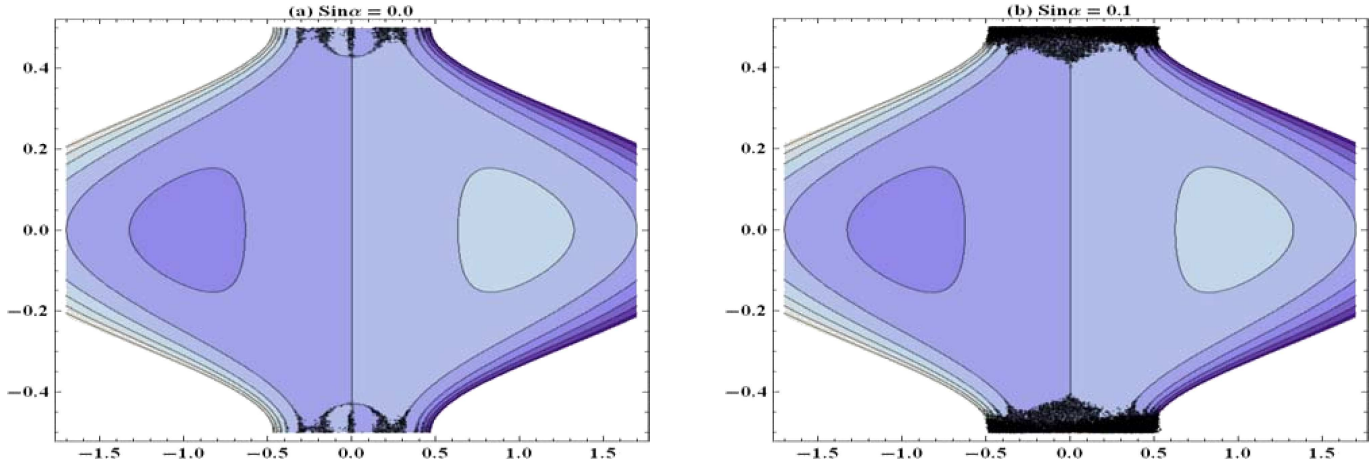

Fig. 7. Streamlines for channel inclination α

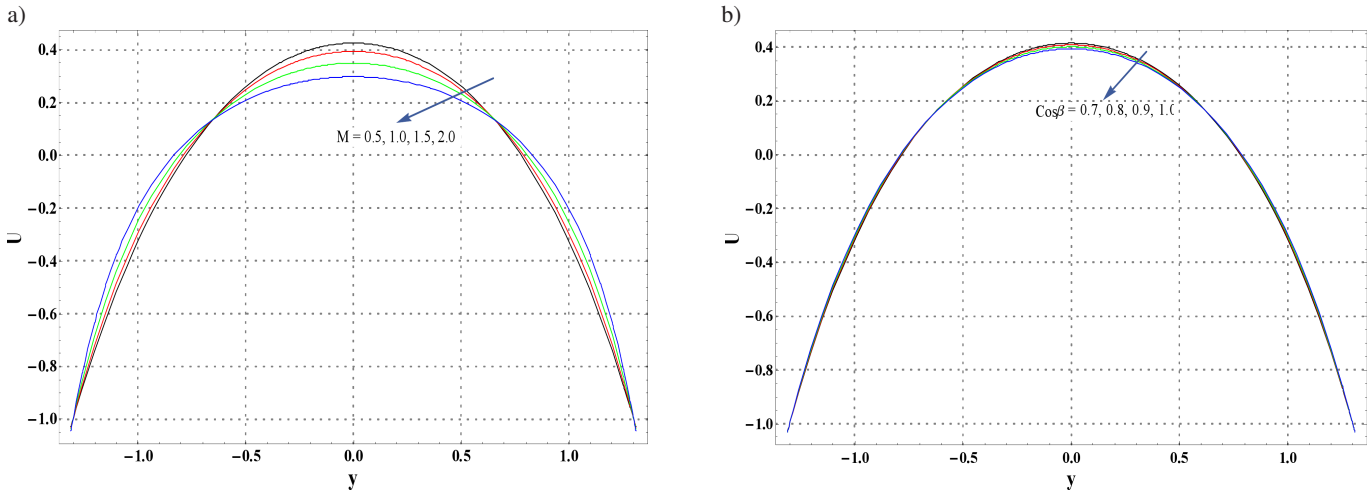

[Fig. 8ab]

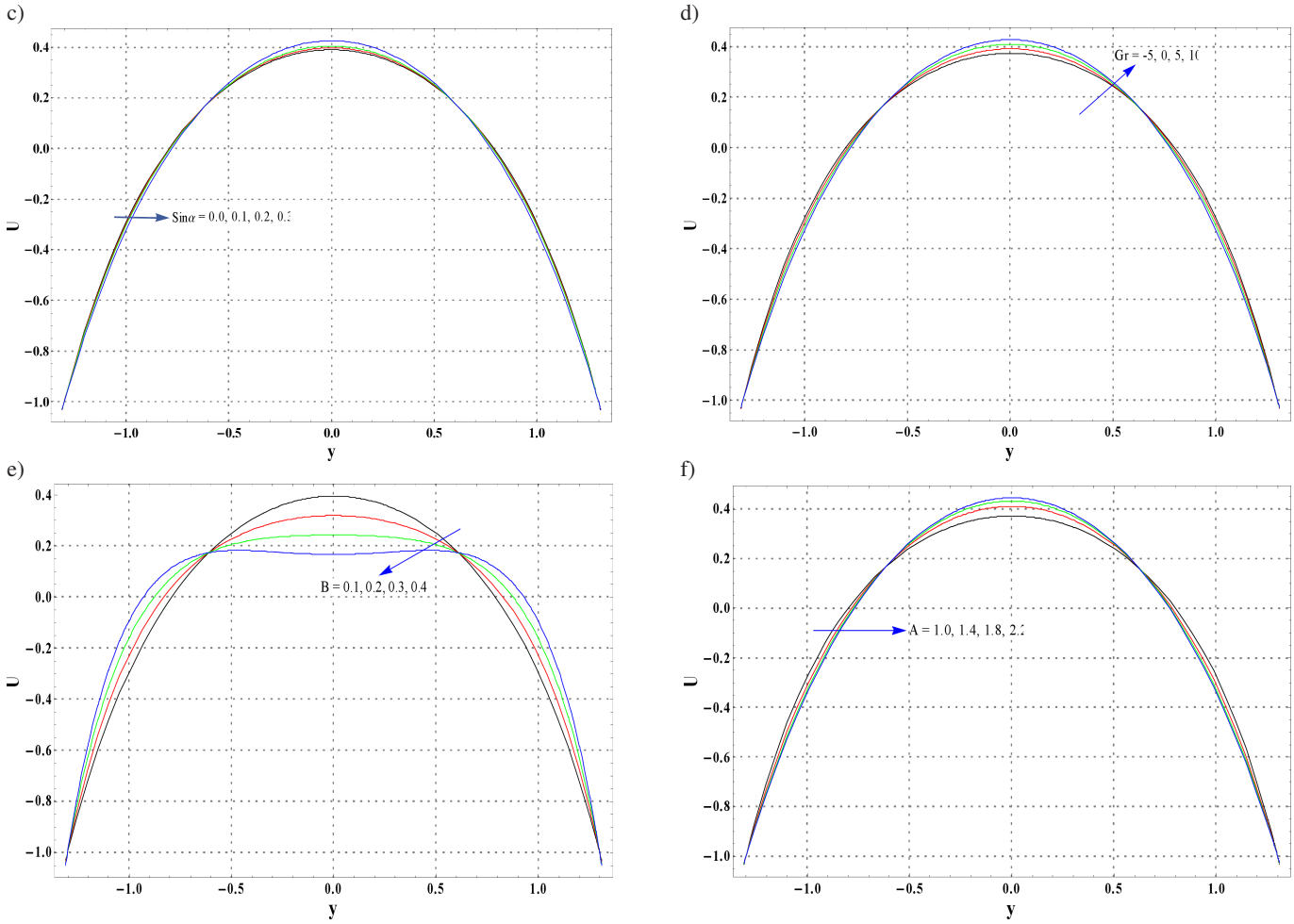

Fig. 8. Longitudnal velocity for various parameters

Behavior of dimensionless temperature is analyzed in Fig. 9. From these figures it is clear that the temperature increases with increase in M, Gr and A but it decreases for β. This highlights the fact that the applied magnetic field has maximum impact on the temperature when it is applied exactly in the normal direction to the channel. The effect of M on temperature is dominant when compared to that of Gr.

Analysis of the Sutterby fluid model

Figure 10 are plotted for the pressure rise in the Sutterby fluid model. It is observed that the Sutterby fluid model exhibits more non-Newtonian behavior than the Eyring-Prandtl fluid model. The graphs of pressure rise are more curved in this case than in the previous case. Variation in the values of parameters brings more abrupt change in case of Sutterby fluid in the retrograde and augmented pumping regions.

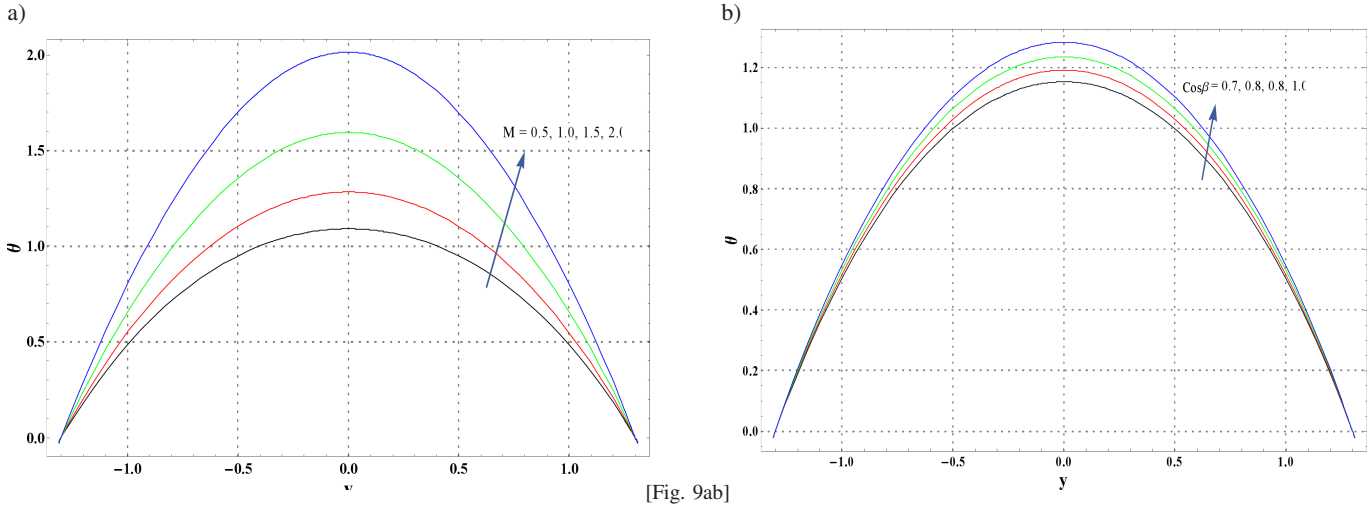

[Fig. 9ab]

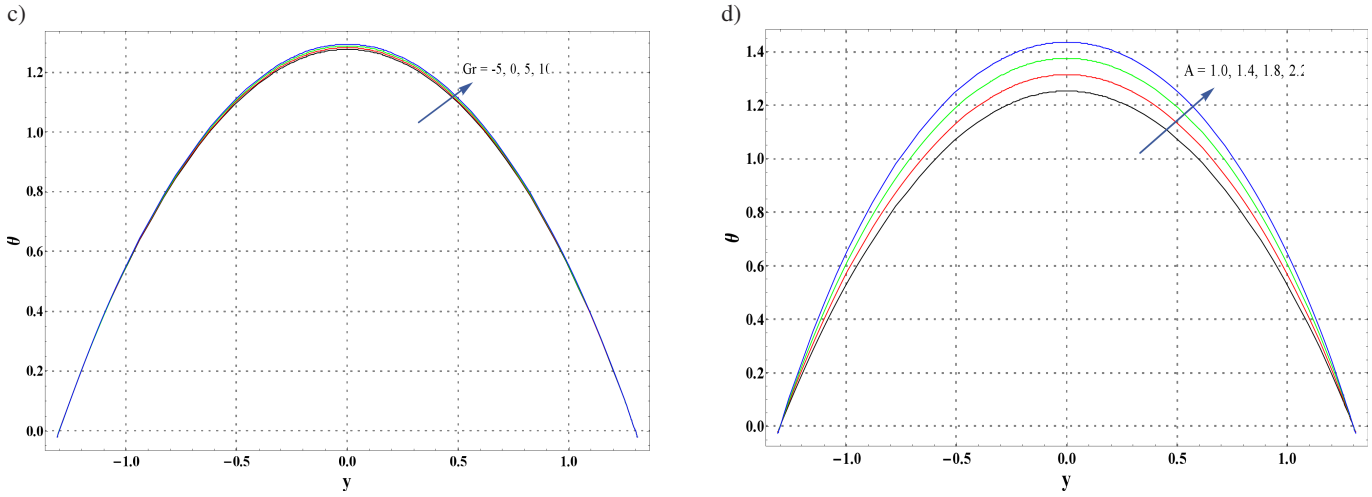

Fig. 9. Dimensionless temperature for several embedded parameters

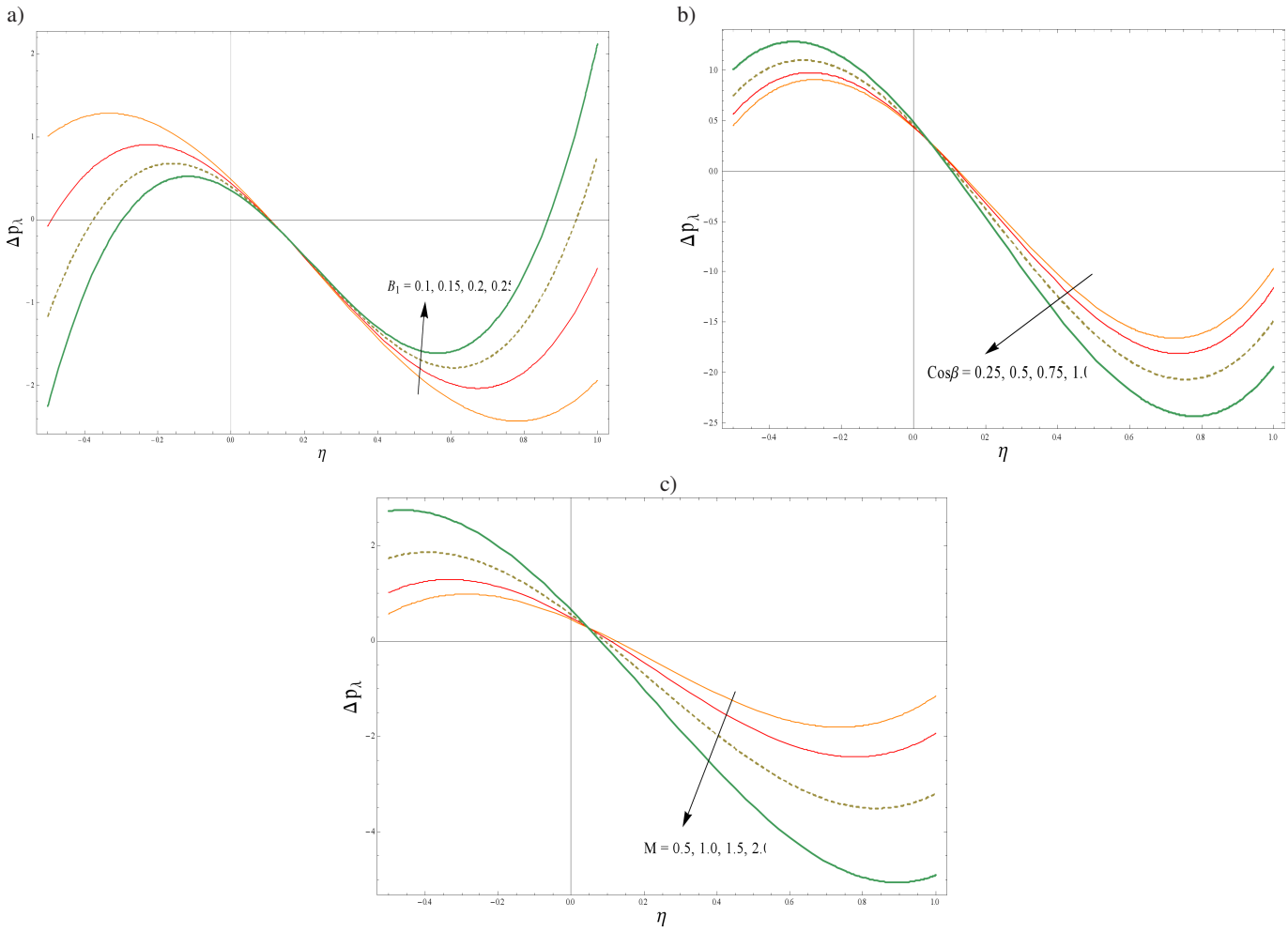

Fig. 10. Pressure rise for several flow parameters

Values attained by the pressure gradient near the wider part of the channel are higher in this case. Qualitatively, the parameters have the same effect on pressure gradient as in the previous case but quantitatively a small variation in the values of the parameters brings a relatively large change in the values of pressure gradient (see Fig. 11). Increase in Hartman number results in decreasing the size of trapped bolus (Figs. 11a,b).

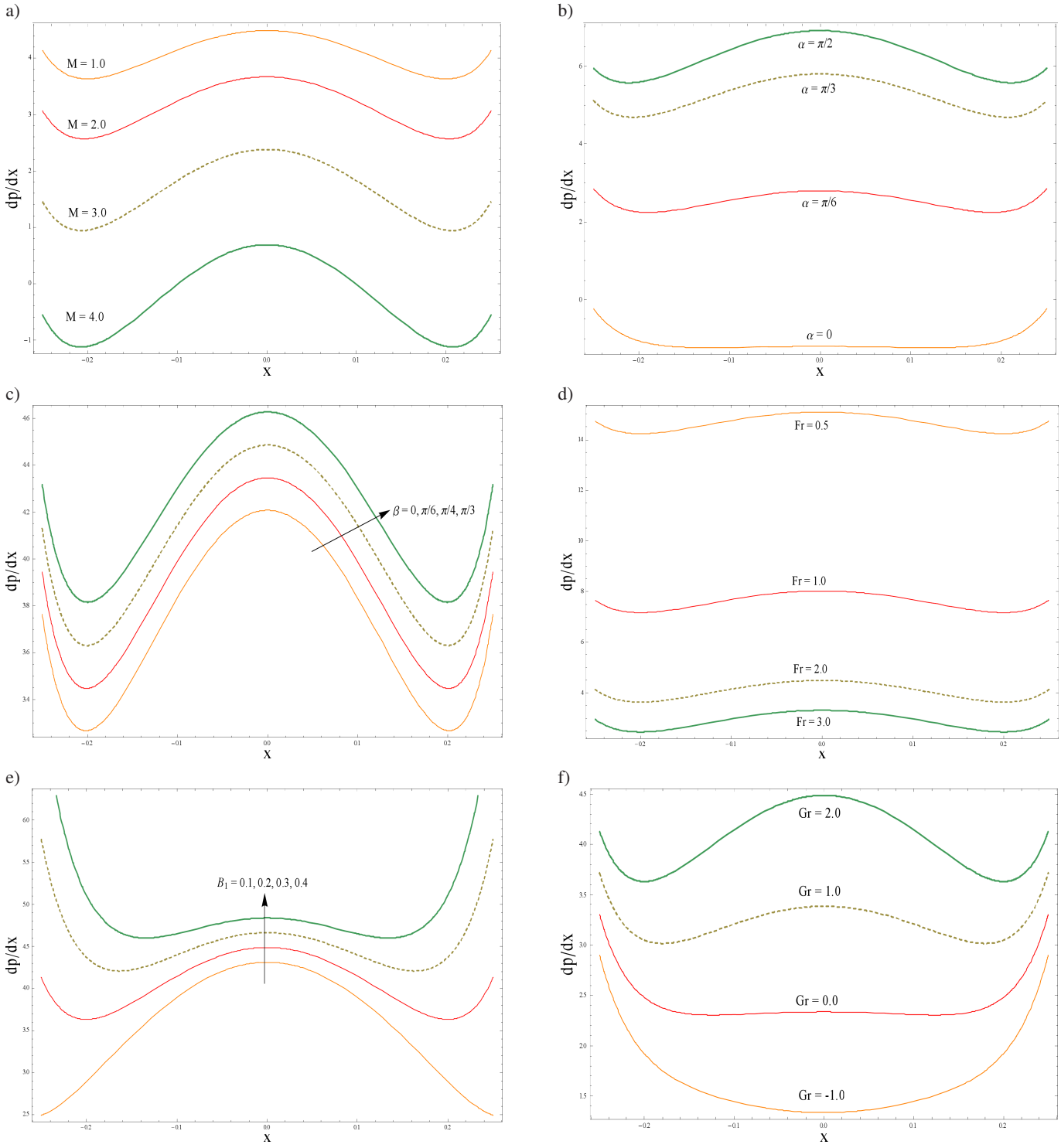

Fig. 11. Variation of pressure gradient

The trapped bolus tends to vanish rapidly in case of Sutterby fluid. The non-Newtonian parameter of this model (B_1) has a considerable large impact on the size of bolus. Even a small increase in the value of B_1 leads to vanish the trapped bolus i.e. trapping in case of Sutterby fluid occurs only for smaller values of B_1 (Fig. 13). Further, increase in α and β increases the size of trapped bolus (see Figs. 14, 15). Behavior of longitudinal velocity and dimensionless temperature is almost similar in the case of Sutterby fluid when compared with the Eyring-Prandtl fluid (see Figs. 16, 17).

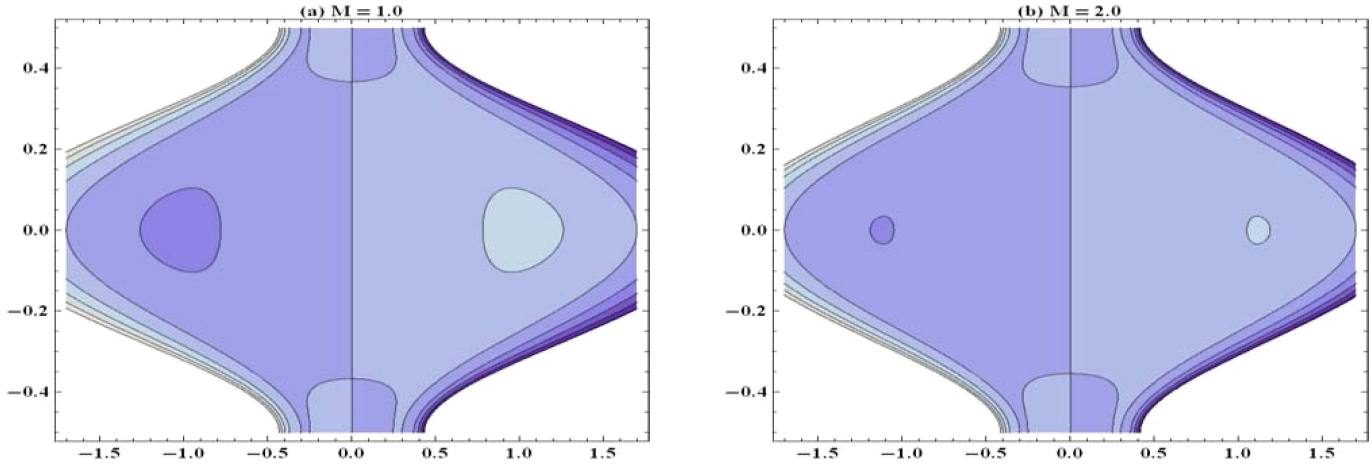

Fig. 12. Streamlines for Hartman number M

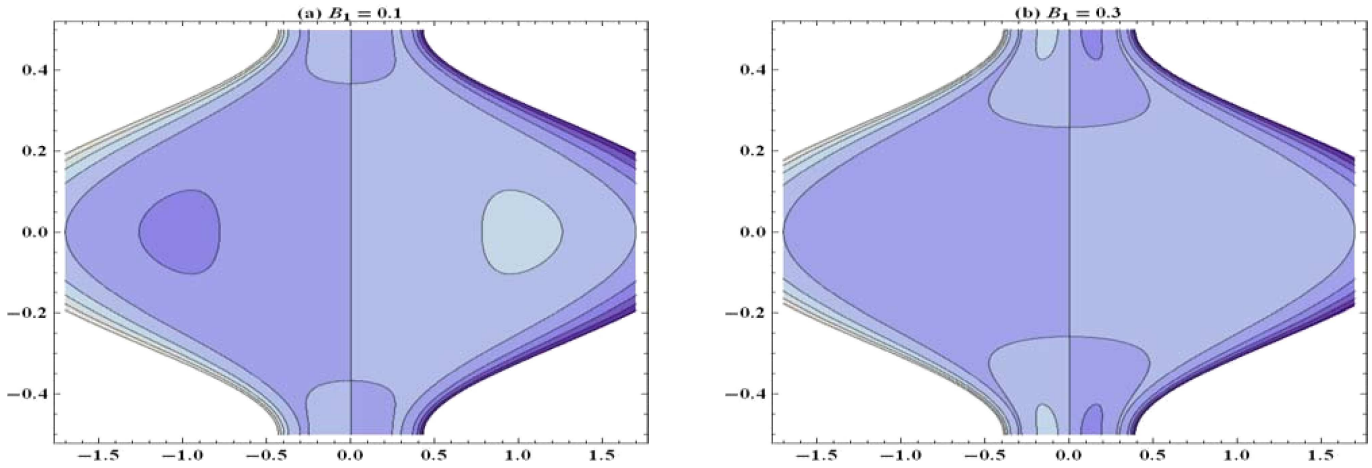

Fig. 13. Streamlines for B_1

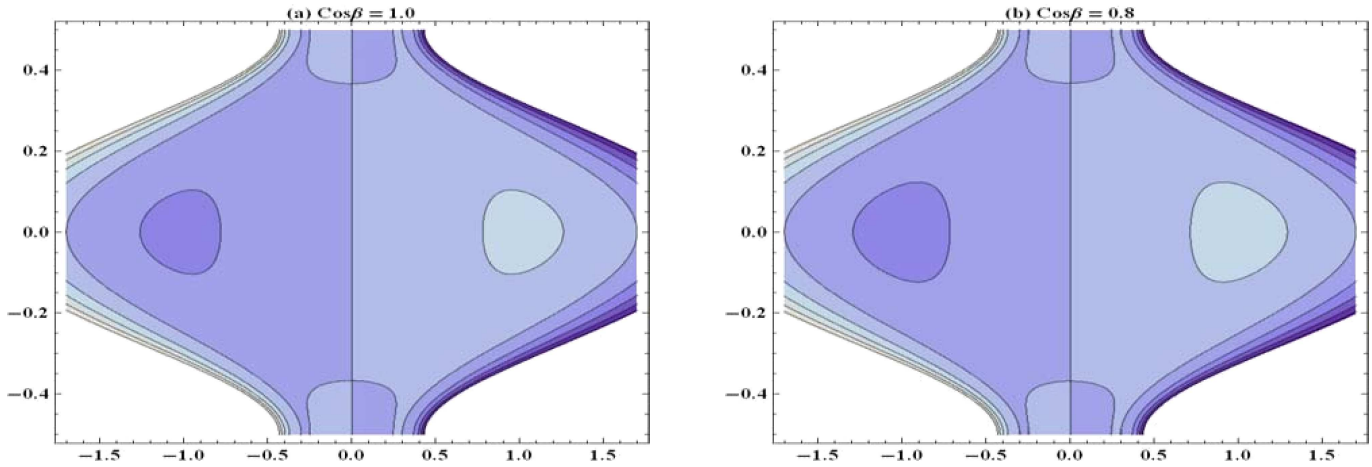

Fig. 14. Streamlines for β

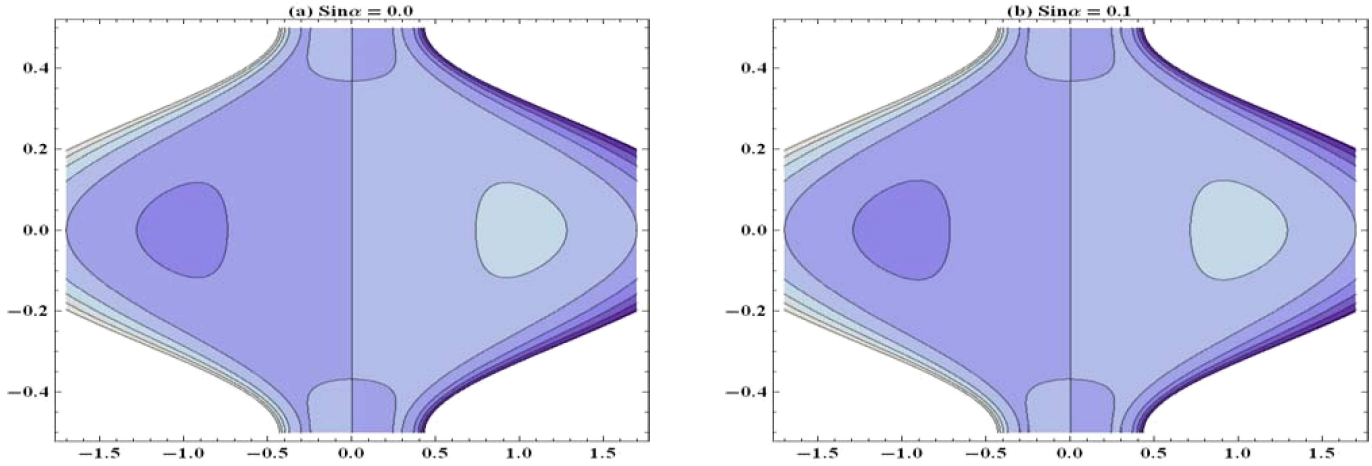

Fig. 15. Streamlines for α

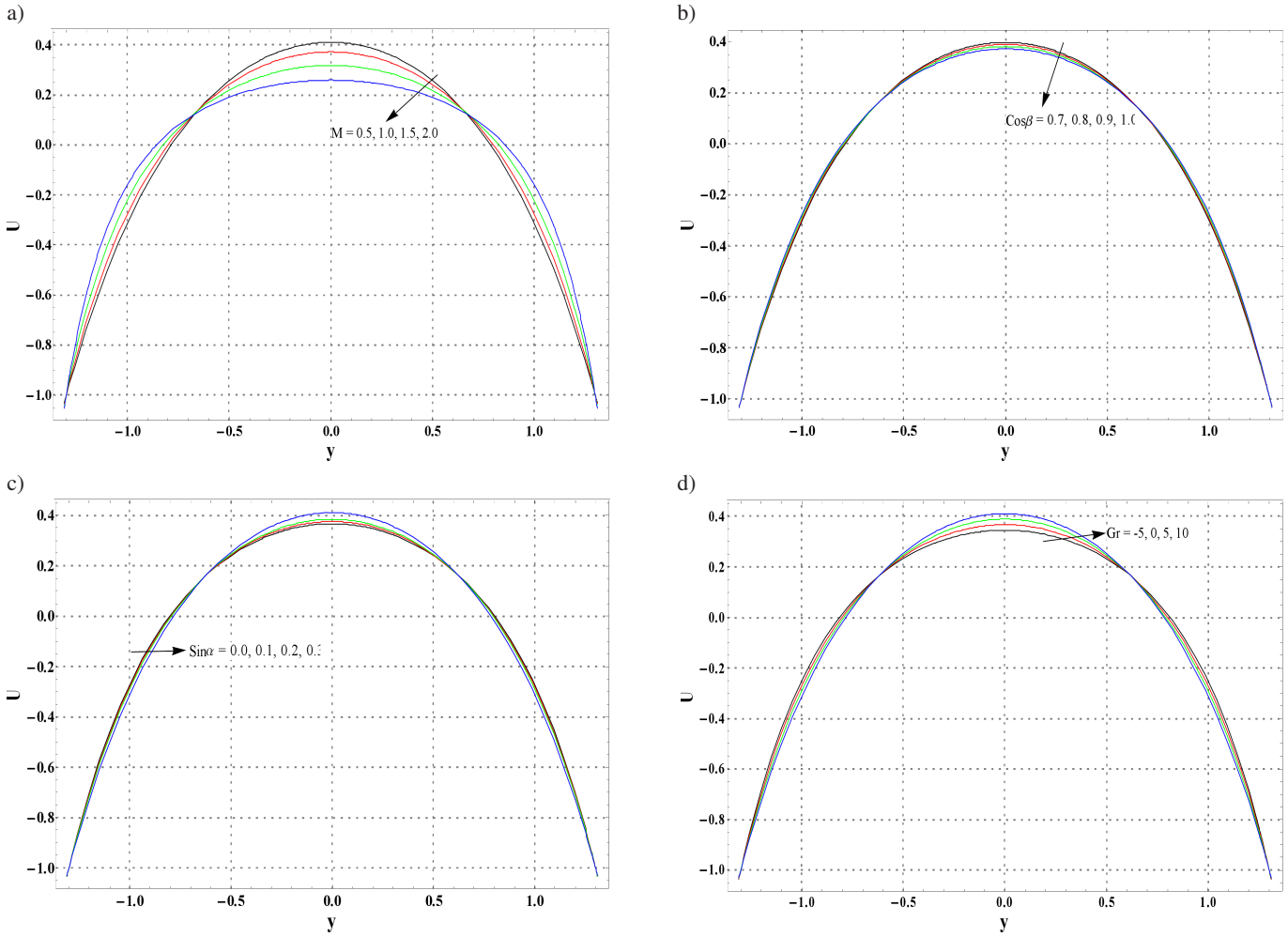

[Fig. 16c-d]

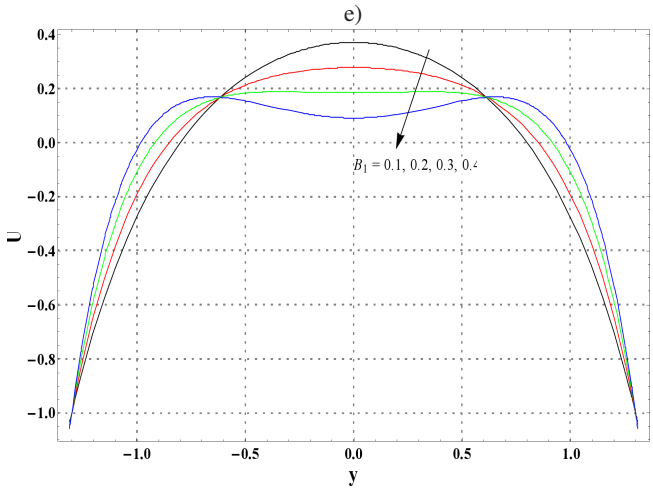

Fig. 16. Longitudnal velocity for several embedded parameters

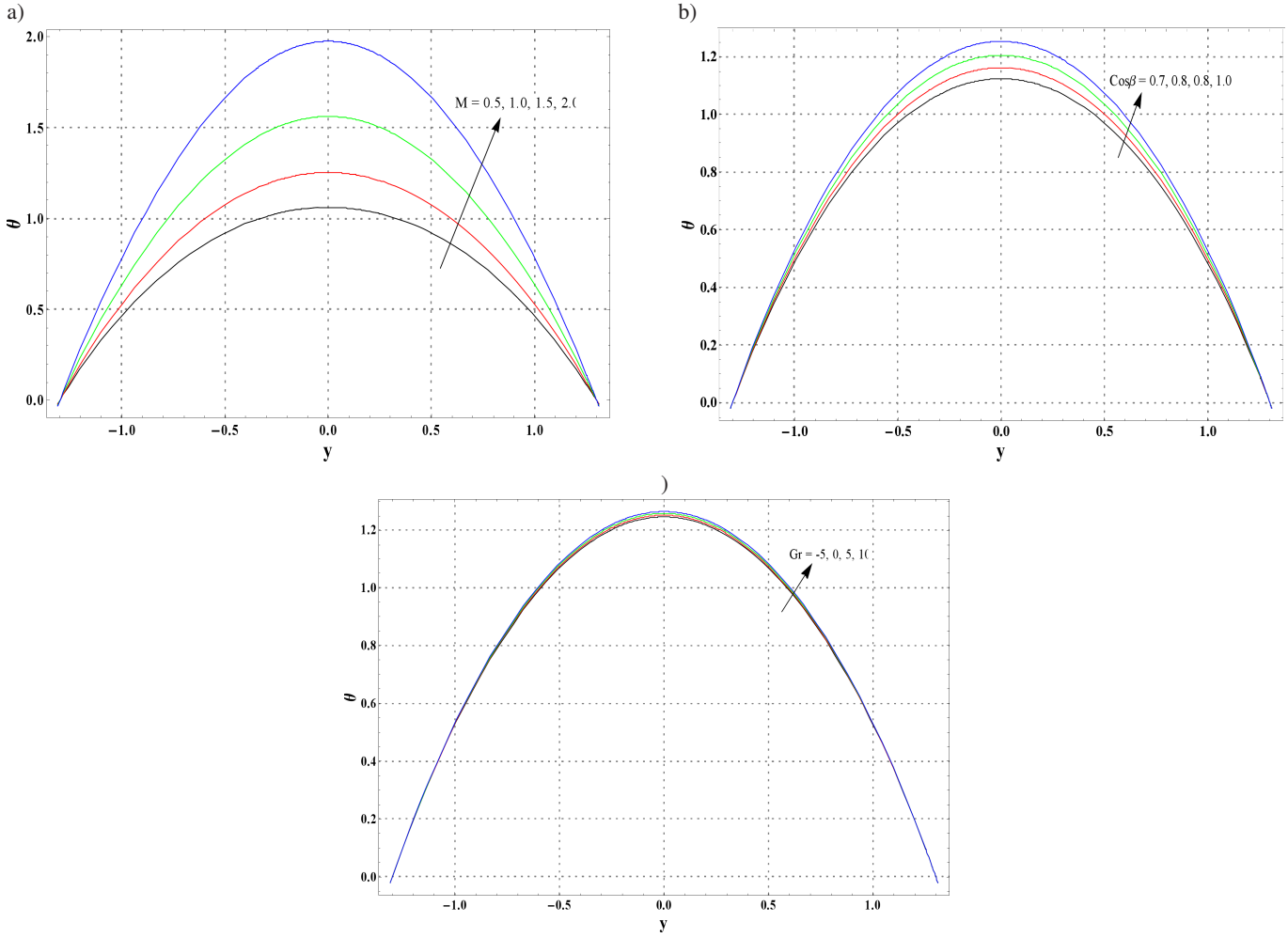

Fig. 17. Variation in dimensionless temperature

Heat transfer rate at the wall and comparison with numerical solution

Numerical values of the heat transfer rate at the wall for both the fluid models are given in the Tables 1 and 2. A comparison with the numerical solutions obtained through Mathematica is also presented in both the tables. The results obtained via perturbation are termed as θ and the numerical results are shown by θ^*. It is found that our results are in

good agreement with the numerical results (up to third decimal) for both the fluid models. It is also seen that the heat transfer rate at the wall increases with increase in M, A and α but it decreases with increase in β. Such an increase in a heat transfer rate for α is very slow when compared with the other parameters. Moreover, the values of a heat transfer rate at the wall are higher for Eyring-Prandtl fluid than for the Sutterby fluid.

Table 1
Numerical values of heat transfer rate for Eyring-Prandtl fluid at h

M	α	β	A	$-\theta'(h_1)$	$-(\theta')^*(h_1)$
0.5	$\frac{\pi}{4}$	$\frac{\pi}{4}$	2	1.35125	1.35041
1.0				1.35746	1.3566
1.5				1.36778	1.36694
2.0				1.38215	1.38133
	0			1.35123	1.35038
	$\frac{\pi}{6}$			1.35124	1.3504
	$\frac{\pi}{4}$			1.35125	1.35046
	$\frac{\pi}{3}$			1.35125	1.3506
		0		1.35332	1.35247
		$\frac{\pi}{6}$		1.35228	1.35144
		$\frac{\pi}{4}$		1.35125	1.35046
		$\frac{\pi}{3}$		1.35021	1.3495
			1.0	1.32668	1.32584
			1.5	1.33896	1.33812
			2.0	1.35125	1.35046
			2.5	1.36353	1.3628

Table 2
Numerical values of heat transfer rate for Sutterby fluid at h

M	α	β	$-\theta'(h_1)$	$-(\theta')^*(h_1)$
0.5	$\frac{\pi}{4}$	$\frac{\pi}{4}$	1.32668	1.32584
1.0			1.33288	1.33199
1.5			1.34314	1.34228
2.0			1.35737	1.35654
	0		1.32665	1.32578
	$\frac{\pi}{6}$		1.32667	1.32582
	$\frac{\pi}{4}$		1.32668	1.32594
	$\frac{\pi}{3}$		1.32669	1.32623
		0	1.32875	1.32789
		$\frac{\pi}{6}$	1.32771	1.32687
		$\frac{\pi}{4}$	1.32668	1.32594
		$\frac{\pi}{3}$	1.32564	1.32506

REFERENCES

[1] T.W. Latham, "Fluid motion in a peristaltic pump", *M. S. Thesis*, Massachusetts Institute of Technology, Cambridge, 1966.

[2] A.H. Shapiro, M.Y. Jaffrin, and S.L. Wienberg, "Peristaltic pumping with long wavelengths at low Reynolds number". *J. Fluid Mech.* 37, 799–825 (1969).

[3] Kh.S. Mekheimer, "Effect of the induced magnetic field on peristaltic flow of a couple stress fluid", *Physics Letters* A, 372 4271–4278 (2008).

[4] M. Kothandapani and S. Srinivas, "Peristaltic transport of a Jeffrey fluid under the effect of magnetic field in an asymmetric channel", *Int. J. Non-Linear Mech.* 43, 915–924 (2008).

[5] N. Ali, T. Hayat, and Y. Wang, "Magnetohydrodynamic peristaltic flow of a third order fluid in an asymmetric channel", *Int. J. Numer. Meth. Fluids* 64, 992–1013 (2010).

[6] N. Ali, M. Sajid, T. Javed, and Z. Abbas, "Heat transfer analysis of peristaltic flow in a curved channel", *Int. J. Heat Mass Transfer* 53, 3319–3325 (2010).

[7] T. Hayat and F.M Abbasi, "Variable viscosity effects on the peristaltic motion of a third order fluid", *Int. J. Numerical Methods in Fluids* 67, 1500–1515 (2011).

[8] T. Hayat, F.M. Abbasi, and A.A. Hendi, "Heat transfer analysis for peristaltic mechanism in variable viscosity fluid", *Chinese Physics Letters* 28, 044701 (2011).

[9] N.S. Gad, "Effect of Hall currents on interaction of pulsatile and peristaltic transport induced flows of a particle-fluid suspension", *Applied Mathematics and Computation* 217, 4313–4320 (2011).

[10] Y. Abd Elmaboud, "Influence of induced magnetic field on peristaltic flow in an annulus", *Communications in Nonlinear Science and Numerical Simulation* 17, 685–698 (2012).

[11] D. Tripathi, "A mathematical model for swallowing of food bolus through the oesophagus under the influence of heat transfer", *Int J. Therm. Sci.* 51, 91–101 (2012).

[12] Kh.S. Mekheimer, S.R. Komy, and S.I. Abdelsalamd, "Simultaneous effects of magnetic field and space porosity on compressible Maxwell fluid transport induced by a surface acoustic wave in a microchannel", *Chin. Phys.* B 22, 124702 (2013).

[13] F.M. Abbasi, T. Hayat, A. Alsaedi and B. Ahmed, "Soret and Dufour effects on peristaltic transport of MHD fluid with variable viscosity", *Appl. Math. Inf. Sci.* 8, 211–219 (2014).

[14] F.M. Abbasi, A. Alsaedi, and T. Hayat, "Peristaltic flow in an asymmetric channel with convective boundary conditions and Joule heating", *J. Cent. South Uni*. 21, 1411–1416 (2014).

[15] T. Hayat, F.M. Abbasi, B. Ahmad, and A. Alsaedi, "MHD mixed convection peristaltic flow with variable viscosity and thermal conductivity", *Sains Malays*. 43, 1583–1590 (2014).

[16] N.S. Akbar, "MHD Eyring-Prandtl fluid flow with convective boundary conditions in small intestines", *Int. J. Biomath*. 6, 1350034 (2013).

[17] N.S. Akbar, "Convective heat transfer of a Sutterby fluid in an inclined asymmetric channel with partial slip", *Heat Transfer Research* 45, 219–240 (2014).

[18] F.M. Abbasi, T. Hayat, and B. Ahmad, "Peristaltic transport of copper-water nanofluid saturating porous medium", *Physica E: Low-dimensional Systems and Nanostructures* 67, 47–53 (2015).

[19] F.M. Abbasi, T. Hayat, and A. Alsaedi, "Peristaltic transport of magneto-nanoparticles submerged in water: model for drug delivery system", *Physica E: Low-dimensional Systems and Nanostructures* 68, 123–132 (2015).